

Facile electrospinning fabrication and photoluminescence of LaOI:Tb³⁺ one-dimensional nanomaterials

Shang Wu · Xiangting Dong · Jinxian Wang ·
Qingling Kong · Wensheng Yu · Guixia Liu

Received: 14 November 2013 / Accepted: 14 December 2013 / Published online: 24 December 2013
© Springer Science+Business Media New York 2013

Abstract LaOI:Tb³⁺ nanomaterials including nanofibers, nanobelts, and hollow nanofibers were successfully synthesized by electrospinning combined with a double-crucible iodination method using NH₄I as iodine source for the first time. X-ray diffractometry analysis revealed that LaOI:Tb³⁺ nanostructures were phase-pure tetragonal structure with space group of P4/nmm. Scanning electron microscopy analysis showed that the diameters of LaOI:Tb³⁺ nanofibers, hollow nanofibers and the width of nanobelts were respectively 199.5 ± 30, 376.05 ± 48 nm and 5.2 ± 1.3 μm under the 95 % confidence level. The thickness of the tubewall for hollow nanofibers was 40.5 nm and the thickness of LaOI:Tb³⁺ nanobelts was 154 nm. Photoluminescence (PL) study demonstrated that the LaOI:Tb³⁺ nanomaterials exhibited the emission peaks located at 485, 544, 583 and 625 nm, which were ascribed to ⁵D₃ → ⁷F_{1, 6}, ⁵D₄ → ⁷F₅, ⁵D₄ → ⁷F₄ and ⁵D₄ → ⁷F₃ of energy level transitions of Tb³⁺, respectively. The PL intensity was strongly affected by the Tb³⁺-doping concentration, and the optimum quenching concentration was 9 %. The luminescence intensity of LaOI:Tb³⁺ nanofibers was obviously stronger than that of LaOI:Tb³⁺ hollow nanofibers and nanobelts under the same measuring conditions. Commission Internationale de L'Eclairage (CIE) analysis demonstrated that the luminescence color of LaOI:9 % Tb³⁺ nanostructures were located in the green region in CIE chromaticity coordinates diagram. The possible formation mechanisms of LaOI:Tb³⁺ one dimensional nanomaterials were also proposed.

1 Introduction

In recent years, rare earth (RE) ions-doped luminescent materials have attracted much attention of the scientists due to their significant advantages, such as low cost, excellent luminescent efficiency, color purity, thermal stability, and good electrochemical performance [1–3]. They have potential applications as light emitting diode (LED) [4–6], laser materials [7, 8], optical signal amplification and fluoroimmunoassay [9]. Terbium ions doped luminescent materials are of both fundamental and technical interest due to their characteristic luminescence properties, such as extremely sharp emission bands, high photochemical stability, long luminescence lifetimes (up to several microseconds), and potential high internal quantum efficiency [10]. So far, many Tb³⁺ doped materials have been synthesized, such as, Y₂O₃:Tb³⁺ [11], LaOBr:Tb³⁺ [12], CaF₂:Ce³⁺/Tb³⁺ [13], Sr₂B₂O₅:Tb³⁺, Li⁺ [14], etc.

Nanofiber, hollow nanofiber and nanobelt are new kinds of one-dimensional nanomaterials with special morphologies. They have attracted increasing interest of scientists owing to their anisotropy, large length-to-diameter ratio and width-to-thickness ratio, unique optical, electrical and magnetic performances [15–23]. Research on the fabrication and properties of nanofibers, hollow nanofibers and nanobelts has become one of the popular subjects of study in the realm of nanomaterials.

Electrospinning is an outstanding technology to process viscous solutions or melts into continuous fibers with diameters ranging from micrometer to submicron or nanometer. This method attracts extensive academic investigations, and is also applied in many areas, such as filtration [24, 25], optical and chemical sensors [26], biological scaffolds [27, 28] and electrode materials [29, 30].

As reported, LaOI could be used as an effective host for rare-earth activators and may have potential application in

S. Wu · X. Dong (✉) · J. Wang · Q. Kong · W. Yu · G. Liu
Key Laboratory of Applied Chemistry and Nanotechnology at
Universities of Jilin Province, Changchun University of Science
and Technology, Changchun 130022, China
e-mail: dongxiangting888@163.com

manufacturing X-ray intensifying screen. So far, LaOI powder has been prepared via direct solid-state reaction at high temperature [31, 32], as follows: La_2O_3 and NH_4I were mixed and reacted in argon flow at 1,000 °C for 10 h [31], or KI and KNO_3 were added into the mixture as cosolvent [32]. Nevertheless, LaOI: Tb^{3+} one-dimensional nanomaterials cannot be easily prepared using this process, if La_2O_3 : Tb^{3+} nanomaterials were directly mixed with NH_4I powders, the nanomaterials will be cut into pieces by the melted NH_4I . Hence, traditional solid-state method is not suitable for prepare LaOI: Tb^{3+} one-dimensional nanostructures, the fabrication of pure-phase LaOI: Tb^{3+} one-dimensional nanostructures remain a challenging and meaningful subject of study.

In this paper, Tb^{3+} -doped La_2O_3 nanofibers, hollow nanofibers, and nanobelts were successfully prepared by calcining the electrospun (PVP)/[$\text{La}(\text{NO}_3)_3 + \text{Tb}(\text{NO}_3)_3$] composites, and LaOI: Tb^{3+} nanofibers, hollow nanofibers, and nanobelts were fabricated by iodination of La_2O_3 : Tb^{3+} one-dimensional nanostructures under argon atmosphere. The morphology, structure and Photoluminescence (PL) properties of the resulting samples were investigated in detail. In addition, the formation mechanism of LaOI: Tb^{3+} nanostructures were also presented.

2 Experimental sections

2.1 Materials

Polyvinyl pyrrolidone (Mw = 90,000 and 10,000, AR), N,N-dimethylformamide (DMF, AR) and ammonium iodide (NH_4I , AR) were purchased from Tianjin Tiantai Chemical Co. Ltd. Lanthanum oxide (La_2O_3 , 99.99 %) and terbium oxide (Tb_4O_7 , 99.99 %) were supplied by China Pharmaceutical Group Shanghai Chemical Reagent Company. Nitric acid (HNO_3 , AR) was bought from Beijing chemical Co. Ltd. All chemicals were directly used as received without further purification.

2.2 Preparation of LaOI: $x\% \text{Tb}^{3+}$ nanofibers

La_2O_3 : $x\% \text{Tb}^{3+}$ [$x = 1, 3, 5, 7, 9$ and 11, x stands for molar ratio of $\text{Tb}^{3+}/(\text{Tb}^{3+} + \text{La}^{3+})$] nanostructures were prepared by calcining the electrospun PVP/[$\text{La}(\text{NO}_3)_3 + \text{Tb}(\text{NO}_3)_3$] composites. In the typical procedure of preparing representative La_2O_3 :9 % Tb^{3+} nanofibers, 0.8184 g of La_2O_3 and 0.0763 g of Tb_4O_7 were dissolved in dilute HNO_3 (1:1, volume ratio) at elevated temperature to form $\text{RE}(\text{NO}_3)_3 \cdot 6\text{H}_2\text{O}$ ($\text{RE} = \text{La}^{3+}, \text{Tb}^{3+}$) through evaporating excess HNO_3 and water from the solution, then the obtained $\text{RE}(\text{NO}_3)_3 \cdot 6\text{H}_2\text{O}$ was dissolved in 16.3996 g of DMF, and then 1.8004 g of PVP (Mw = 90,000) was added into the

above solution under stirring for 4 h to form homogeneous transparent spinning solution. In spinning solution, the mass ratio of PVP, RE nitrate and DMF was 9:9:82. Subsequently, the PVP/[$\text{La}(\text{NO}_3)_3 + \text{Tb}(\text{NO}_3)_3$] composite nanofibers were obtained by electrospinning of the spinning solution at room temperature under the direct current high-voltage of 12.4 kV, and the distance between the spinneret and collector was fixed at 20 cm. Finally, La_2O_3 :9 % Tb^{3+} nanofibers were prepared by calcining PVP/[$\text{La}(\text{NO}_3)_3 + \text{Tb}(\text{NO}_3)_3$] composite nanofibers at 700 °C for 8 h with a heating rate of 1 °C/min in air. LaOI:9 % Tb^{3+} nanofibers can be prepared by iodating La_2O_3 :9 % Tb^{3+} nanofibers with NH_4I as iodization agent, described as following: La_2O_3 :9 % Tb^{3+} nanofibers were loaded into a small crucible, then the small crucible was placed into a big crucible, and then excessive NH_4I was added into the space between the two crucibles, the big crucible was covered with its lid. Then the samples were annealed at 800 °C for 4 h with a heating rate of 2 °C/min under argon atmosphere, the iodization temperature was decreased to 200 °C at a rate of 2 °C/min, and then down to room temperature naturally. Thus, LaOI:9 % Tb^{3+} nanofibers were successfully acquired. Other series of LaOI: $x\% \text{Tb}^{3+}$ ($x = 1, 3, 5, 7$ and 11) of nanofibers were prepared by the similar procedure except for different doping concentration of Tb^{3+} ions.

2.3 Fabrication of LaOI:9 % Tb^{3+} nanobelts and hollow nanofibers

LaOI:9 % Tb^{3+} nanobelts and hollow nanofibers were also formed by adjusting the ratios of inorganic salts, DMF, PVP and the electrospinning parameters in the above procedures. The molecular weight of PVP added into the spinning solution for preparing nanobelts and hollow nanofibers were 90,000 and 10,000, respectively. The compositions of spinning solutions and the experimental conditions were summarized in Table 1. Other processes of preparations followed the same procedures of preparation for LaOI:9 % Tb^{3+} nanofibers, as described in the Sect. 2.2.

3 Characterization

X-ray diffraction (XRD) measurements were carried out using a Rigaku D/max-RA X-ray diffractometer with Cu K α radiation of 0.15406 nm. The morphologies and sizes of the samples were investigated by an XL-30 field emission scanning electron microscope (SEM) made by FEI Company. The purity of the products was examined by an Oxford ISIS-300 energy dispersive spectrometer (EDS). PL measurements of samples were recorded on a Hitachi F-7000 fluorescence spectrophotometer using an Xe lamp

Table 1 Compositions of the spinning solutions and conditions of electrospinning

Sample	Nitrates (g)	PVP (g)	DMF (g)	Stirring time (h)	Voltage (kV)	Distance (cm)	Room Temperature (°C)	Relative humidity (%)
Nanofibers	1.8	1.8	16.4	4	12.4	20	20–25	25–40
Nanobelts	1.8	3.6	12.6	12	8.0	16	20–25	35–50
Hollow nanofibers	1.8	4.2	6	12	13.0	18	18–25	50–70

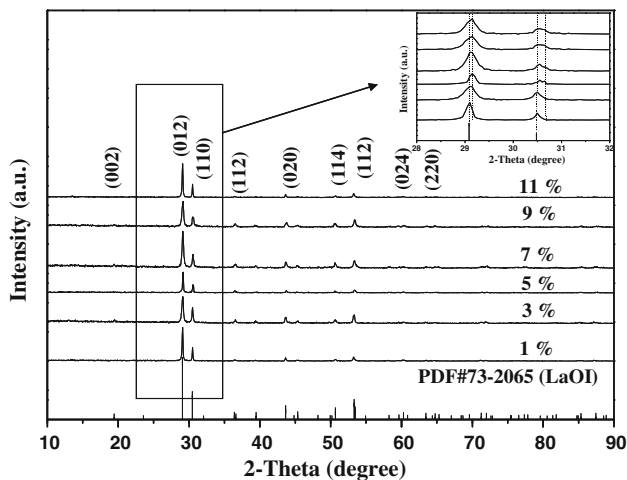


Fig. 1 XRD patterns of LaOI: x %Tb³⁺ nanofibers (x = 1, 3, 5, 7, 9 and 11) with PDF standard card of LaOI

as the excitation source. The specific surface areas of the nanostructures were measured by a V-Sorb 2800P specific surface area and pore size analyzer made by Gold App Instrument Co. Ltd.

4 Results and discussion

4.1 Crystal structure

Figure 1 shows the XRD patterns of the LaOI nanofibers doped with different molar concentration of Tb³⁺ ions. As seen from Fig. 1, well-defined diffraction peaks are acquired, all of which can be readily indexed to those of the pure phase LaOI with tetragonal structure according to the PDF standard card No.73-2065 (LaOI) and the space group is P4/nm, the characteristic diffraction peaks are located near 2θ = 29.15°, 30.55°, 36.5°, 45.3°, 43.8°, 50.6° and 53.35°. No diffraction peaks of any other phases or impurities are detected, indicating that La³⁺ ions may be substituted by Tb³⁺ ions successfully to form the luminescence centre because of the similar radius between La³⁺ ions and Tb³⁺ ions [radius(La³⁺) = 0.106 nm, radius(Tb³⁺) = 0.092 nm]. However, the diffraction peaks of LaOI:x %Tb³⁺ nanofibers slightly shift, as seen from the inset of Fig. 1, meaning that the lattice constants of LaOI:x %Tb³⁺ nanostructures will

Table 2 Lattice constants of LaOI:x %Tb³⁺ (x = 1, 3, 5, 7, 9 and 11) nanofibers

X	2-Theta (°)	h	k	l	Lattice constants (Å)
1	29.1	0	1	2	a = b = 4.1416
	30.5	1	1	0	c = 9.1225
3	29.1	0	1	2	a = b = 4.1416
	30.5	1	1	0	c = 9.1225
5	29.15	0	1	2	a = b = 4.1350
	30.55	1	1	0	c = 9.1061
7	29.1	0	1	2	a = b = 4.1305
	30.55	1	1	0	c = 9.1400
9	29.15	0	1	2	a = b = 4.1416
	30.5	1	1	0	c = 9.0886
11	29.15	0	1	2	a = b = 4.1305
	30.55	1	1	0	c = 9.1061

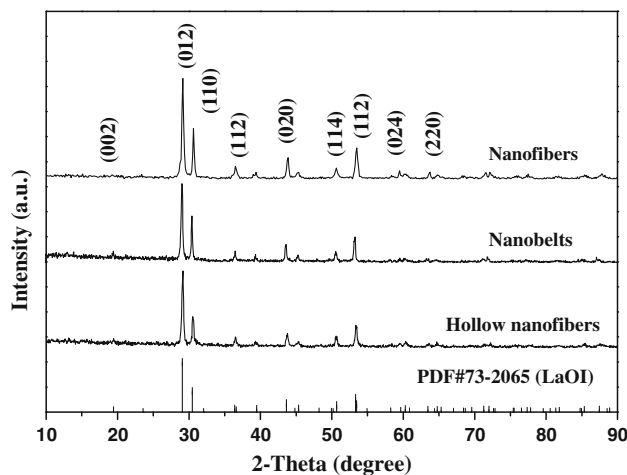


Fig. 2 XRD patterns of LaOI:9 %Tb³⁺ nanofibers, nanobelts and hollow nanofibers with PDF standard card of LaOI

be slightly changed. The lattice constants were calculated using the following expression:

$$\sin^2\theta = (\lambda/2a)^2 \times (h^2 + k^2) + (\lambda/2c)^2 \times l^2 \tag{1}$$

where λ value is 1.5406 Å, h, k and l are diffraction indexes. The results are summarized in Table 2. The similar structures were obtained for the LaOI:9 %Tb³⁺

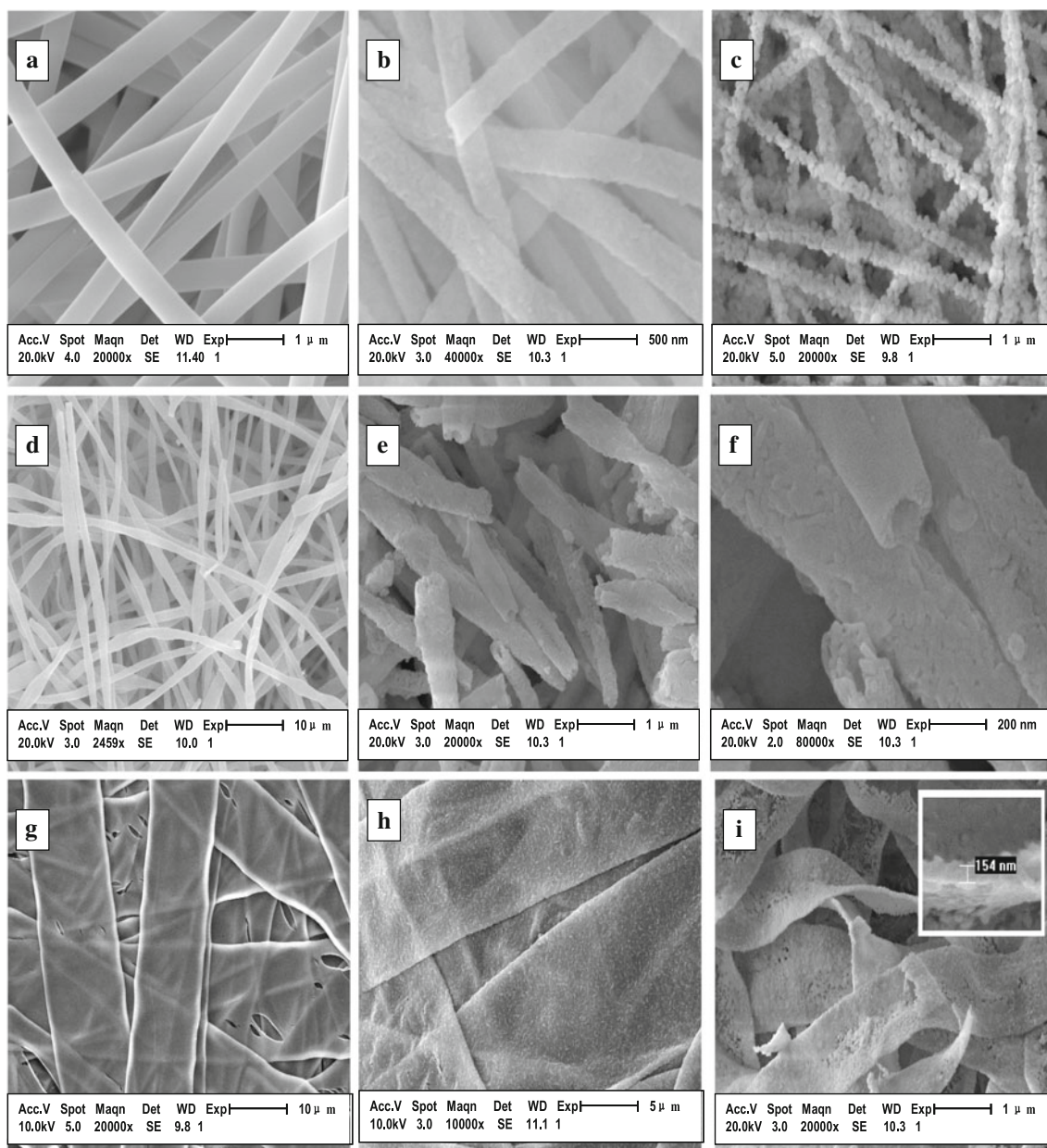


Fig. 3 SEM images of [PVP/[La(NO₃)₃ + Tb(NO₃)₃] composite nanofibers (PVP Mw = 90,000) (a), La₂O₃:9 %Tb³⁺ nanofibers (b), LaOI:9 %Tb³⁺ nanofibers (c), [PVP/[La(NO₃)₃ + Tb(NO₃)₃] composite nanofibers (PVP Mw = 10,000) (d), La₂O₃:9 %Tb³⁺ hollow

nanofibers (e), LaOI:9 %Tb³⁺ hollow nanofibers (f), [PVP/[La(NO₃)₃ + Tb(NO₃)₃] composite nanobelts (g), La₂O₃:9 %Tb³⁺ hollow nanobelts (h), and LaOI:9 %Tb³⁺ nanobelts (i)

nanofibers, nanobelts and hollow nanofibers, as manifested in Fig. 2. It is found that the diffraction angles do not change, indicating that they have same structures.

4.2 Morphology

Figure 3a, d, g show SEM images of PVP/[La(NO₃)₃ + Tb(NO₃)₃] composite nanostructures, respectively. As seen from the images, the nanostructures have smooth surface. After annealing at 800 °C, as-formed La₂O₃:9 %Tb³⁺

nanofibers, hollow nanofibers and nanobelts have relatively smooth surface, as shown in Fig. 3b, e, h. Meanwhile, one can see that the hollow nanofibers exhibit hollow-centered fibrous structure. Figure 3c, f, i manifest the SEM images of LaOI:9 %Tb³⁺ nanofibers, hollow nanofibers and nanobelts, they have coarse surface. Under the 95 % confidence level, the diameters of those nanofibers and hollow nanofibers, the width of the nanobelts analyzed by Shapiro–Wilk method are normal distribution. Histograms of diameters and width distribution of the nanostructures are

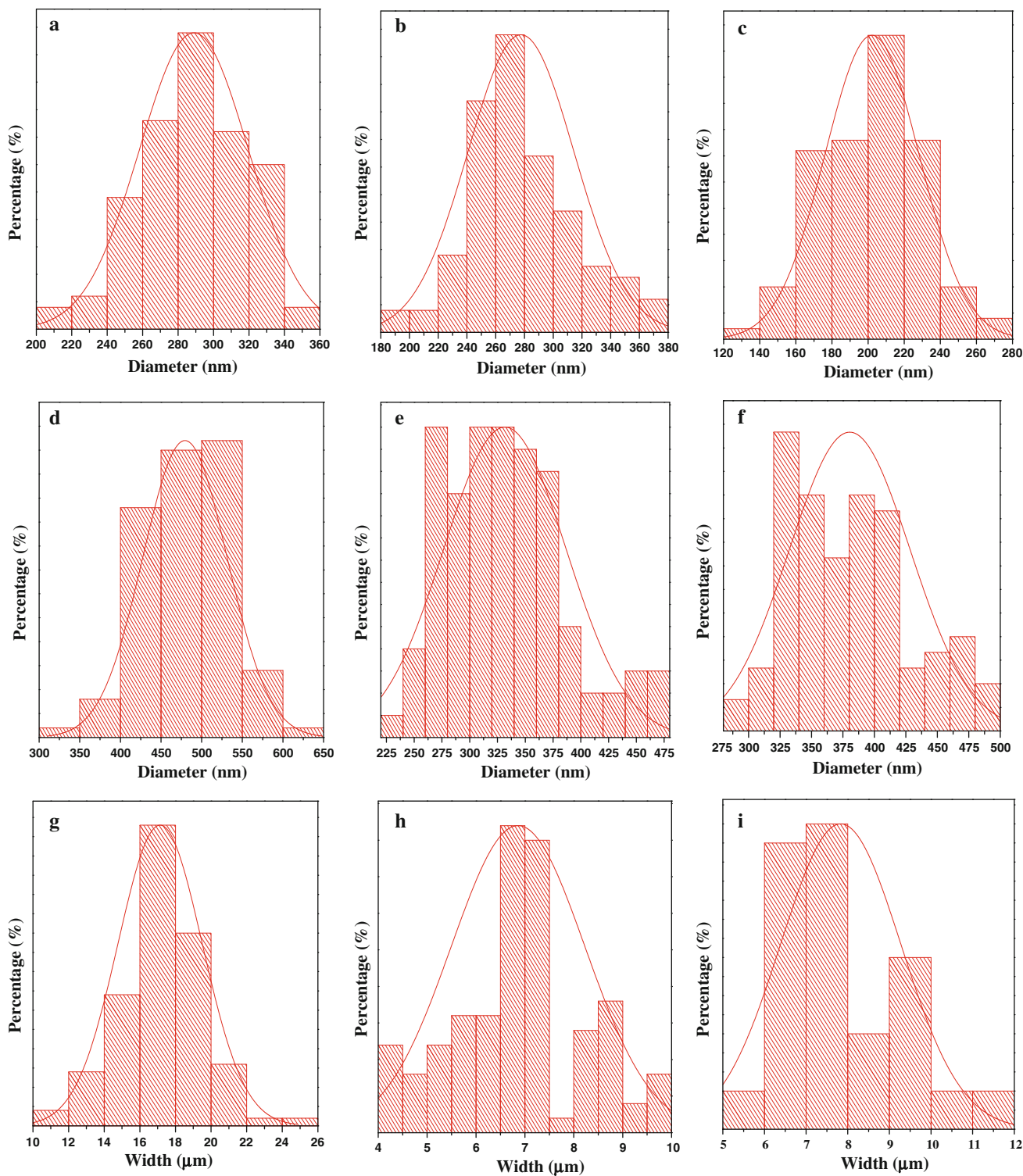


Fig. 4 Histograms of diameter distribution of [PVP/[La(NO₃)₃ + Tb(NO₃)₃] composite nanofibers (PVP Mw = 90,000) (a), La₂O₃:9 %Tb³⁺ nanofibers (b), LaOI:9 %Tb³⁺ nanofibers (c), [PVP/[La(NO₃)₃ + Tb(NO₃)₃] composite nanofibers (PVP Mw = 10,000) (d), La₂O₃:9 %Tb³⁺ hollow nanofibers (e), LaOI:9 %Tb³⁺ hollow nanofibers (f), and width distribution histograms of [PVP/[La(NO₃)₃ + Tb(NO₃)₃] composite nanobelts (g), La₂O₃:9 %Tb³⁺ nanobelts (h), and LaOI:9 %Tb³⁺ nanobelts (i)

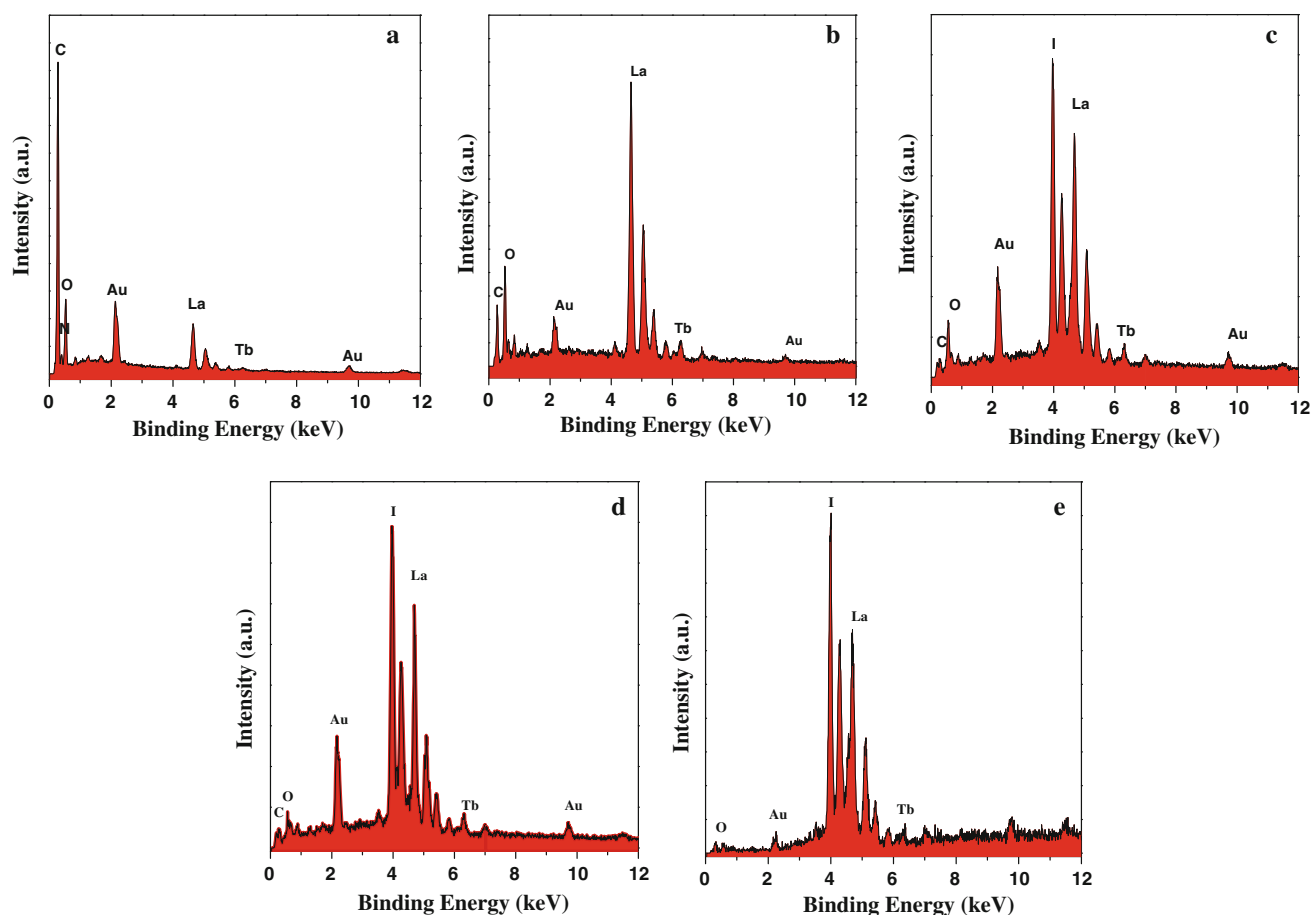


Fig. 5 EDS spectra of PVP/[La(NO₃)₃ + Tb(NO₃)₃] composite nanofibers (a), La₂O₃:9 %Tb³⁺ nanofibers (b), LaOI:9 %Tb³⁺ nanofibers (c), LaOI:9 %Tb³⁺ hollow nanofibers (d) and LaOI:9 %Tb³⁺ nanobelts (e)

shown in Fig. 4. As seen from Fig. 4, the diameters of LaOI:9 %Tb³⁺ nanofibers, hollow nanofibers and the width of LaOI:9 %Tb³⁺ nanobelts are 199.5 ± 30 , 376.05 ± 48 nm and 5.2 ± 1.3 μ m, respectively. SEM images show, after the iodization, the diameter of LaOI:9 %Tb³⁺ nanofibers is smaller than that of La₂O₃:9 %Tb³⁺ nanofibers [33], and the surface of LaOI:9 %Tb³⁺ nanofibers is coarser than La₂O₃:9 %Tb³⁺ nanofibers. The thickness of the LaOI:Tb³⁺ nanobelts and the tubewall thickness of the hollow nanofibers are 154 and 40.5 nm, respectively.

4.3 Energy dispersive spectrum analysis

EDS spectra of [La(NO₃)₃ + Tb(NO₃)₃]/PVP, La₂O₃:9 %Tb³⁺, LaOI:9 %Tb³⁺ nanofibers, hollow nanofibers and nanobelts are shown in Fig. 5. EDS spectra show that C, N, O, La and Tb are main elements in composite nanofibers, C, O, La and Tb in La₂O₃:9 %Tb³⁺ nanofibers, C, O, I, La, and Tb elements in LaOI:Tb³⁺ nanofibers and hollow nanofibers, and O, I, La, and Tb elements in LaOI:Tb³⁺ nanobelts. In the LaOI:9 %Tb³⁺ nanofibers and hollow nanofibers, C element comes from the used carbon rod. The peak of Au is from the conductive film of

Au plated on the sample. The [La(NO₃)₃ + Tb(NO₃)₃]/PVP and La₂O₃:9 %Tb³⁺ hollow nanofibers and nanobelts have the similar EDS spectra compared with the nanofibers. No other elements are found in the samples, indicating that the LaOI:9 %Tb³⁺ nanostructures are highly pure.

4.4 Photoluminescence properties

Figure 6 shows the PL excitation (monitored by 544 nm) and emission (excited by 264 nm) spectra of the LaOI:9 %Tb³⁺ nanofibers. As seen from Fig. 6a, the excitation spectrum exhibits two broad bands in the range from 210 nm to 280 nm. The weak broadband at about 217 nm is due to the spin-allowed transition from 4f⁸ configuration to 4f⁷5d configuration of Tb³⁺ ions. The strong broadband at ca. 264 nm is assigned to the spin-forbidden transition of Tb³⁺ ions. It is found from Fig. 6b that the emission spectrum consists of six main peaks at 417, 439, 485, 544, 583, and 625 nm, which originate from the ⁵D₃ → ⁷F_J (J = 5, 4) and ⁵D₄ → ⁷F_J (J = 6, 5, 4, 3) transitions of Tb³⁺ ions, respectively. Among these emission peaks, the green emission at 544 nm attributed to

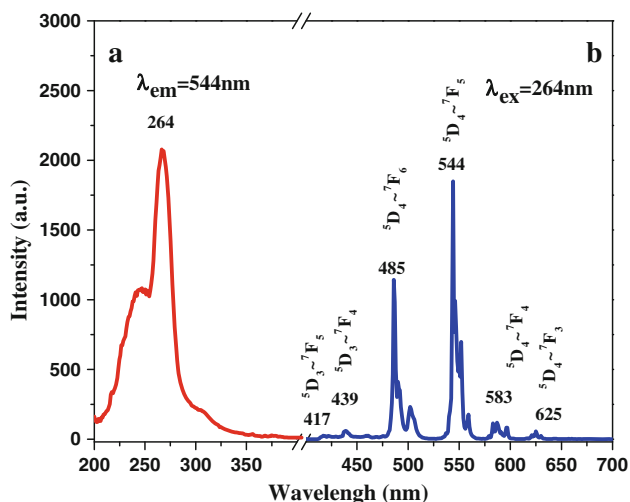


Fig. 6 Excitation (a) and emission (b) spectra of LaOI:9 %Tb³⁺ nanofibers

⁵D₄ → ⁷F₅ energy level transition of Tb³⁺ ions is the strongest one. As shown in Fig. 7, the spectral shape and position of excitation and emission peaks do not vary with the doping concentrations of Tb³⁺ ions for LaOI:x %Tb³⁺ nanofibers, but the intensity of excitation and emission peaks for LaOI:x %Tb³⁺ nanofibers strongly depends on the doping concentration of Tb³⁺ ions and the strongest excitation and emission spectra can be obtained when the doping molar concentration of Tb³⁺ ions is 9 %. Obviously, the luminescence intensity of LaOI:Tb³⁺ nanofibers is increased with the increase of the concentration of Tb³⁺ ions from the beginning, reaches a maximum value with the Tb³⁺ ions concentration of 9 %, and then decreases with the further increase in Tb³⁺ concentration, indicated that the optimum molar concentration of Tb³⁺ ions is 9 %. As shown in Fig. 8, the PL decay curves of LaOI:x %Tb³⁺ nanofibers with different concentration of Tb³⁺ ions (1, 3, 5, 7, 9, and 11 %), are used to calculate the lifetime and to investigate the luminescence dynamics of these samples. All the samples are excited by 264 nm and monitored at 544 nm. The curves follow the single-exponential decay:

$$I_t = I_0 \exp(-t / \tau) \tag{2}$$

In the above formula, I_t is the intensity at time t, I₀ is the intensity at t = 0, and τ is the decay lifetime. The corresponding luminescence lifetime values of LaOI:x %Tb³⁺ nanofibers are 1.45, 1.57, 1.66, 1.52, 1.61, and 1.67 ms corresponding to the Tb³⁺ concentration of 1, 3, 5, 7, 9 and 11 %, respectively.

Figure 9 demonstrates the comparisons among the emission spectra and excitation spectra of the LaOI:9 %Tb³⁺ nanostructures with different morphologies measured under the same conditions. From Fig. 9, one can see that LaOI:9 %Tb³⁺ nanofibers have higher PL intensity than that of hollow nanofibers and nanobelts. The result can be

interpreted by two diverse factors. Generally, the crystallinity of materials has a crucial impact on the luminescence intensity, the higher the crystallinity, the stronger the PL intensity. The order of the crystallinity of the nanomaterials is nanofibers, nanobelts then hollow nanofibers. Therefore, the sequence of PL intensity is nanofibers, nanobelts then hollow nanofibers. It is known that the specific surface area of materials increases with the decrease of size [34]. A large number of defects are introduced into LaOI:9 %Tb³⁺ nanostructures due to the large surface area. Defects as quenching centers have severe drawbacks in luminescence intensity for nanomaterials because they provide nonradiative recombination centers for electrons and holes [35]. The specific surface areas of the LaOI:9 %Tb³⁺ nanofibers, nanobelts and hollow nanofibers determined by BET method were 4.53, 16.41 and 24.56 m²/g, respectively. Therefore, LaOI:9 %Tb³⁺ nanofibers have the smallest quantity of defects due to the smallest specific surface area, as a result, the nanofibers have the strongest PL intensity, in the similar way, the hollow nanofibers have the weakest PL intensity.

As shown in Fig. 10, the PL decay curves of LaOI:9 %Tb³⁺ nanostructures are used to calculate the lifetime and to investigate the luminescence dynamics of these samples. All the samples are excited by 264 nm and monitored at 544 nm. The curves follow the single-exponential decay as formula (2). The corresponding fluorescence lifetime values of LaOI:9 %Tb³⁺ nanofibers, nanobelts, and hollow nanofibers are 1.61, 1.83, and 1.90 ms, respectively.

In general, color can be represented by the Commission Internationale de L’Eclairage (CIE) 1931 chromaticity coordinates. Figure 11a shows the chromaticity coordinates of LaOI:1 %Tb³⁺ (0.181, 0.204), LaOI:3 %Tb³⁺ (0.205, 0.321), LaOI:5 %Tb³⁺ (0.245, 0.495), LaOI:7 %Tb³⁺ (0.235, 0.458), LaOI:9 %Tb³⁺ (0.249, 0.527) and LaOI:11 %Tb³⁺ (0.253, 0.547) nanofibers. Among these nanofibers, LaOI:1 %Tb³⁺ and LaOI:3 %Tb³⁺ nanofibers show nearly blue emission owing to the presence of stronger emission arising from ⁵D₃ → ⁷F_j transitions of Tb³⁺ ions. The chromaticity coordinates of LaOI:9 %Tb³⁺ nanofibers (0.249, 0.527), nanobelts (0.256, 0.560), and hollow nanofibers (0.257, 0.560) are represented in Fig. 11b. They exhibit green emissions. These results indicate that the color emissions can be tuned by changing the concentration of doping activator ions and the morphologies of nanomaterials. These as-obtained nanostructures could show merits of green emissions, which is considered to be a promising candidate for application in LEDs.

4.5 Formation mechanism for LaOI:Tb³⁺ nanostructures

Formation mechanisms of LaOI:Tb³⁺ nanostructures are shown in Fig. 12. In the processes (1) and (2), La(NO₃)₃, Tb(NO₃)₃ and PVP (Mw = 90,000) were mixed with DMF

Fig. 7 Excitation (a) and emission (b) spectra of LaOI:*x* %Tb³⁺ nanofibers (*x* = 1, 3, 5, 7, 9 and 11)

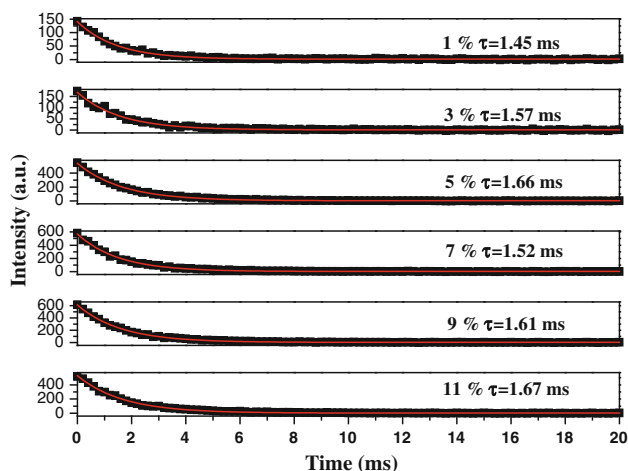
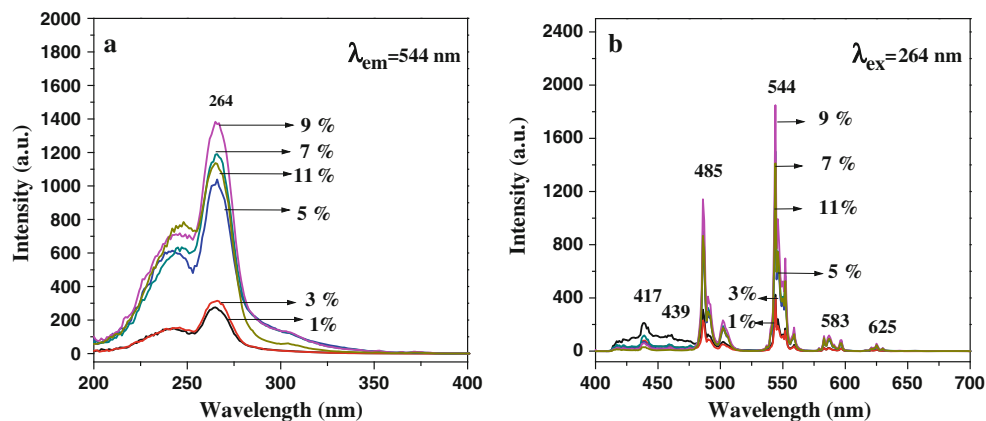


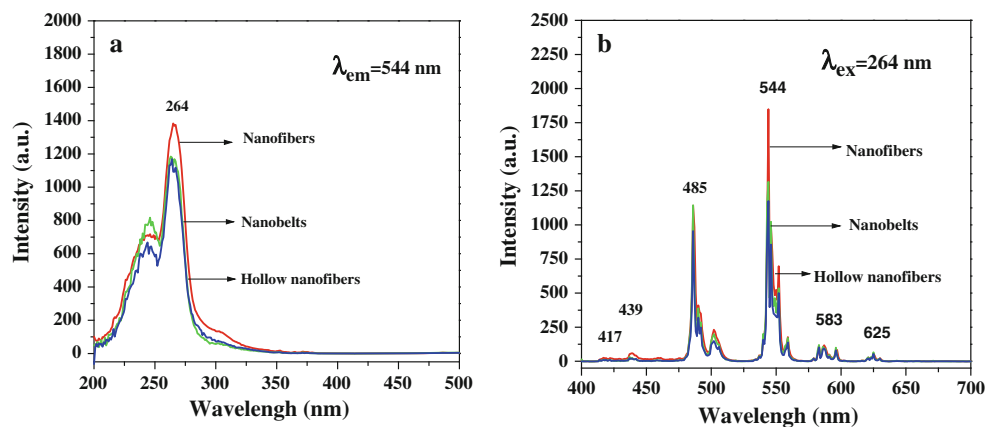
Fig. 8 PL decay curves of LaOI:*x* %Tb³⁺ nanofibers (*x* = 1, 3, 5, 7, 9 and 11)

to form spinning solution with certain viscosity. PVP acted as template during the formation of PVP/[La(NO₃)₃ + Tb(NO₃)₃] composite nanofibers and nanobelts. La³⁺, Tb³⁺ and NO₃⁻ were mixed or absorbed onto PVP to form composite nanofibers and nanobelts via electrospinning. Some solvent was volatilized in the electrospinning

process. PVP, NO₃⁻ and residual solvent were decomposed and eventually evaporated from the composite fibers and belts during the calcinations process. With the increase in the calcining temperature, La³⁺/Tb³⁺ can combine with O₂, coming from air, to form La₂O₃:Tb³⁺ crystallites, and then many crystallites combined into nanoparticles, and finally these nanoparticles mutually connected to generate La₂O₃:Tb³⁺ nanofibers and nanobelts.

It is different that the molecular weight of PVP is 10,000 in the fabrication of the hollow nanofibers. When the PVP/[La(NO₃)₃ + Tb(NO₃)₃] composite nanofibers were heated at high temperature, DMF containing anions and cations in the composite nanofibers would remove to the surface of the fibers, and eventually evaporate from the composite fibers. Thus, the anions and cations also removed to the surface of the composite fibers. With the increase of calcination temperature, PVP, NO₃⁻ would oxidize, and La₂O₃:Tb³⁺ crystallites were formed on the surface of fibers. Many crystallites combined into nanoparticles, which mutually connected to generate La₂O₃:Tb³⁺ hollow nanofibers. We notice that similar formation behaviors of hollow nanofibers have also been observed when the hollow nanofibers of other materials were prepared via monoaxial electrospinning [36], implying that this

Fig. 9 Excitation (a) and emission (b) spectra of LaOI:9 %Tb³⁺ nanofibers, nanobelts and hollow nanofibers



formation mechanism is of universality. By comparing formation process of $\text{La}_2\text{O}_3:\text{Tb}^{3+}$ nanofibers, nanobelts and hollow nanofibers, we found that the morphologies and

sizes of nanostructures prepared by electrospinning can be controlled by adjusting molecular weight of PVP and experimental conditions, such as the precursor solution viscosity, relative air humidity, the structure of spinneret, spinning voltage, and the distance between the spinneret and the collector.

$\text{La}_2\text{O}_3:\text{Tb}^{3+}$ nanostructures were iodinated using NH_4I as iodination agent. In the iodinated process, NH_4I decomposed into NH_3 and HI at about 450°C . With the increase of calcination temperature, HI gases react with $\text{La}_2\text{O}_3:\text{Tb}^{3+}$ nanomaterials to produce $\text{LaOI}:\text{Tb}^{3+}$ nanomaterials. During the process, NH_4I powders and $\text{La}_2\text{O}_3:\text{Tb}^{3+}$ nanomaterials were separated by carbon rods which prevented $\text{La}_2\text{O}_3:\text{Tb}^{3+}$ nanomaterials from morphology damage. If $\text{La}_2\text{O}_3:\text{Tb}^{3+}$ nanostructures were directly mixed with NH_4I powders, the nanostructures will be cut into pieces by the melted NH_4I . The double-crucible method we proposed here is actually a solid–gas reaction, which has been proved to be an important method, not only can retain the morphology of $\text{La}_2\text{O}_3:\text{Tb}^{3+}$ nanomaterials,

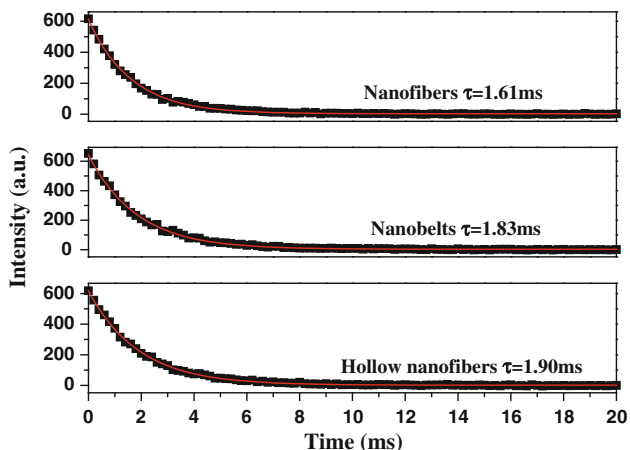


Fig. 10 PL decay curves of $\text{LaOI}:\text{Tb}^{3+}$ nanofibers, nanobelts and hollow nanofibers

Fig. 11 CIE chromaticity coordinates diagrams for $\text{LaOI}:\text{x}\% \text{Tb}^{3+}$ nanofibers ($\text{x} = 1, 3, 5, 7, 9$ and 11) (a) and $\text{LaOI}:\text{Tb}^{3+}$ hollow nanofibers, nanofibers and nanobelts (b)

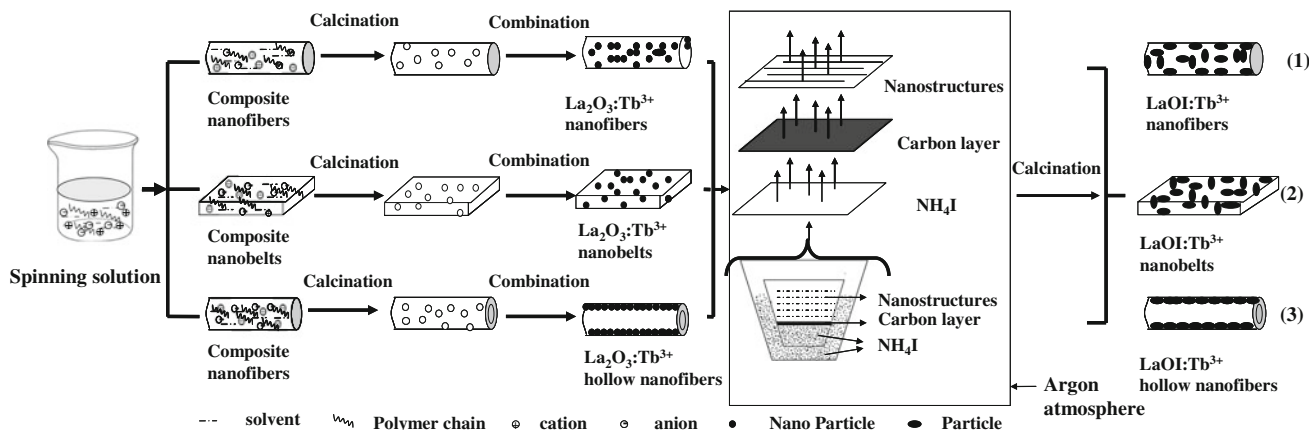
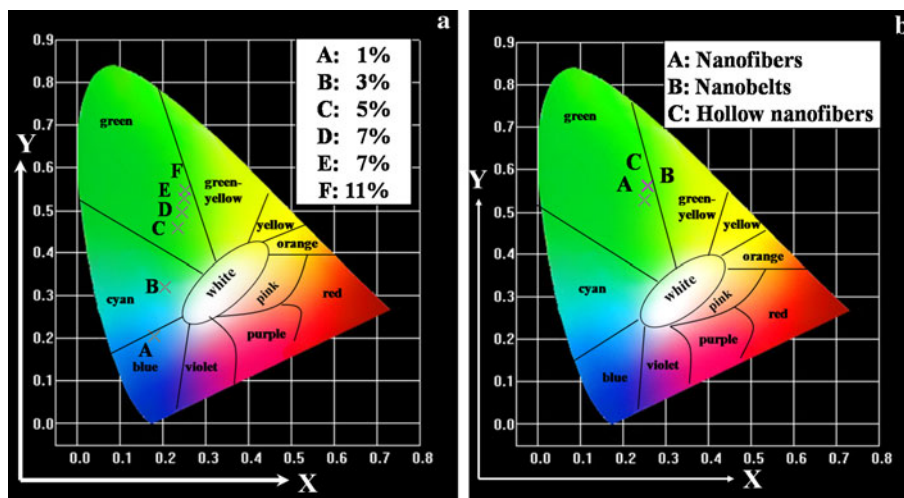
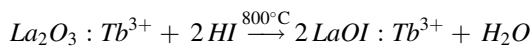
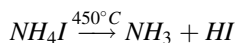
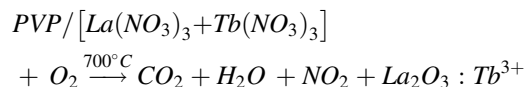


Fig. 12 Schematic diagram of formation mechanism of $\text{LaOI}:\text{Tb}^{3+}$ nanofibers, nanobelts and hollow nanofibers

but also can fabricate LaOI:Tb³⁺ nanomaterials with pure phase at relatively low temperature. Reaction schemes for formation of LaOI:Tb³⁺ nanomaterials proceed as follows:



5 Conclusions

Tb³⁺-doped LaOI nanostructures were synthesized by electrospinning method combined with a double-crucible iodating method using NH₄I as iodination agent. The diameters of the nanofibers and hollow nanofibers respectively are 206.52 ± 30 and 376.05 ± 48 nm, the width and thickness of nanobelts respectively are 5.2 ± 1.3 μm and 154 nm. Under the excitation of 264-nm ultraviolet light, LaOI:9 % Tb³⁺ nanostructures exhibit the characteristic emissions of predominant peak at 544 nm ascribed to ⁵D₄ → ⁷F₅ energy level transition of Tb³⁺ ions. The luminescence intensity of nanofibers is obviously greater than that of hollow nanofibers and nanobelts under the same measuring conditions. The color emissions of LaOI:Tb³⁺ nanostructures can be tuned by changing the concentration of Tb³⁺ ions and the morphologies of nanomaterials.

Acknowledgments This work was financially supported by the National Natural Science Foundation of China (NSFC 50972020, 51072026), Ph.D. Programs Foundation of the Ministry of Education of China (20102216110002, 20112216120003), the Science and Technology Development Planning Project of Jilin Province (Grant Nos. 20130101001JC, 20070402, 20060504), the Science and Technology Research Project of the Education Department of Jilin Province during the eleventh five-year plan period (Under Grant No. 2010JYT01), Key Research Project of Science and Technology of Ministry of Education of China (Grant No. 207026).

References

- L.H. Gao, Y. An, H.L. Zhu, L. Wang, J.J. Chen, N.Y. Wang, G.F. Ou, *J. Mater. Sci.* **46**, 1337–1340 (2011)
- G.G. Li, C.X. Li, Z.Y. Hou, C. Peng, Z.Y. Cheng, J. Lin, *Opt. Lett.* **34**, 3833–3835 (2009)
- M. Kubus, D. Ensling, T. Jüstel, H. Meyer, *Eur. J. Inorg. Chem.* **18**, 1–7 (2013)
- C.F. Zhu, X.L. Liang, Y.X. Yang, G.R. Chen, *J. Lumin.* **130**, 74–77 (2010)
- A.S. Gouveia-Neto, A.F. da Silva, L.A. Bueno, E.B. da Costa, *J. Lumin.* **132**, 299–304 (2012)
- C.H. Huang, T.M. Chen, *J. Phys. Chem. C* **119**, 2349–2355 (2011)
- A. Jha, B. Richards, G. Jose, T.T. Fernandez, P. Joshi, X. Jiang, J. Lousteau, *Prog. Mater. Sci.* **57**, 1426–1491 (2012)
- S. Mirov, V. Fedorov, I. Moskalev, D. Martyshev, C. Kim, *Laser Photonics Rev.* **4**, 21–41 (2009)
- H.X. Cui, J.M. Chen, H.D. Zhou, *Inorg. Chem. Commun.* **10**, 772–775 (2007)
- S.P. Mondejar, A. Kovtun, M. Epple, *J. Mater. Chem.* **17**, 4153–4159 (2007)
- Soichiro. Tsujimoto, Keisuke. Yasuda, Toshiyuki. Masui, Nobuhito. Imanaka, *Adv. Chem. Sci.* **3**, 1928–1936 (2013)
- W.W. Ma, X.T. Dong, J.X. Wang, W.S. Yu, G.X. Liu, *J. Mater. Sci.* **48**, 2557–2565 (2013)
- Y.L. Dai, C.M. Zhang, Z.Y. Cheng, P.A. Ma, C.X. Li, X.J. Kang, D.M. Yang, *J. Lin* **33**, 2583–2592 (2012)
- R. Wang, J. Xu, C. Chen, *Mater. Lett.* **68**, 307–309 (2012)
- J.X. Wang, H.R. Che, X.T. Dong, L. Liu, G.X. Liu, *Acta Opt. Sin.* **30**, 473–479 (2010)
- Q.Z. Cui, X.T. Dong, J.X. Wang, M. Li, *J. Rare Earths* **26**, 664–669 (2008)
- L.Y. Yang, J.X. Wang, X.T. Dong, G.X. Liu, W.S. Yu, *J. Mater. Sci.* **48**, 644–650 (2013)
- Q.L. Ma, J.X. Wang, X.T. Dong, W.S. Yu, G.X. Liu, J. Xu, *J. Mater. Chem.* **22**, 14438–14442 (2012)
- Q.L. Ma, J.X. Wang, X.T. Dong, W.S. Yu, G.X. Liu, *Chem. Eng. J.* **222**, 16–22 (2013)
- H.Y.P. Wang, Y. Yang, Y. Wang, Y.Y. Zhao, X. Li, C. Wang, *J. Nanosci. Nanotechnol.* **9**, 1522–1525 (2009)
- D. Li, X.T. Dong, W.S. Yu, J.X. Wang, G.X. Liu, *J. Mater. Sci.: Mater. Electron.* **24**, 3041–3048 (2013)
- W.S. Yu, Q.L. Kong, J.X. Wang, X.T. Dong, G.X. Liu, *J. Mater. Sci.: Mater. Electron.*, doi:10.1007/s10854-013-1547-x (2013)
- D.Q. Shao, J.X. Wang, X.T. Dong, W.S. Yu, G.X. Liu, F.F. Zhang, L.M. Wang, *J. Mater. Sci.: Mater. Electron.* **24**(12), 4718–4724 (2013)
- L.W. Huang, S.S. Manickam, J.R. McCutcheon, *J. Membrane Sci.* **436**, 213–220 (2013)
- A.F. Lubambo, R.A. de Freitas, M.R. Sierakowski, N. Lucyszyn, G.L. Sasaki, B.M. Serafim, C.K. Saul, *Carbohydr. Polym.* **93**, 484–491 (2013)
- J.M. Corres, Y.R. Garcia, F.J. Arregui, I.R. Matias, *IEEE Sens. J.* **11**, 2383–2387 (2011)
- Suwan.N. Jayasinghe, *Adv. Chem. Phys.* **138**, 2215–2223 (2013)
- B. Zou, Y.W. Liu, X.M. Luo, F. Chen, X.Q. Guo, X.H. Li, *Acta Biomater.* **8**, 1576–1585 (2012)
- Y. Mizuno, E. Hosono, T. Saito, M. Okubo, D.N. Hamane, K.O. Ishi, T. Kudo, H.S. Zhou, *J. Phys. Chem.* **116**, 10774–10780 (2012)
- G.J. Wei, J.G. Liu, H. Zhao, C.W. Yan, *J. Power Sources* **241**, 709–717 (2013)
- Y.D. Eagleman, E.B. Courchesne, S.E. Derenzo, *J. Lumin.* **131**, 669–675 (2011)
- Y.M. Li, H.D. Lu, J.W. Li, X.G. Miao, *J. Lumin.* **35**, 107–110 (1986)
- D. Li, X.T. Dong, W.S. Yu, J.X. Wang, G.X. Liu, *J. Nano. Res.* **15**(6), 1–10 (2013)
- K. Kömpe, O. Lehmann, M. Haase, *Chem. Mater.* **18**, 4442 (2006)
- J. Yang, C.X. Li, Z.W. Quan, C.M. Zhang, P.P. Yang, Y.Y. Li, C.C. Yu, J. Lin, *J. Phys. Chem. C* **112**, 12777 (2008)
- J.X. Wang, H.R. Che, X.T. Dong, G.X. Liu, *Acta Optica Sinica* **30**, 473–479 (2010)